Alexandria Engineering Journal 104 (2024) 235–245

Contents lists available at ScienceDirect

Alexandria Engineering Journal

journal homepage: www.elsevier.com/locate/aej

Original article

Single-fed Ku/Ka dual-band aperture shared planar antenna array for satellite communication

Jeong-Wook Kim [a], Seung-Won Oh [b], Han Lim Lee [b,*]

[a] Department of Electrical and Computer Engineering, Ajou University, Suwon 16499, South Korea
[b] School of Electrical and Electronics Engineering, Chung-Ang University, Seoul, 06974, South Korea

ARTICLE INFO

Keywords:
Satellite communication
Shared-aperture antenna
Circular polarization
Single-fed Ku/Ka dual-band antenna

ABSTRACT

This paper presents a single-fed Ku/Ka dual-band aperture-shared planar antenna array designed for satellite communication. The need to enhance data transmission speeds has driven the exploration of higher frequency bands, such as the Ku-band and Ka-band. Researchers have been investigating the design of multiband antennas to achieve space miniaturization and cost-effectiveness in these higher frequency bands. However, previous works faced challenges, including spatial efficiency limitations, complex radiator structures, band isolation issues, and increased complexity in the feeding network. To address the abovementioned challenges, this paper proposes a single-fed Ku/Ka dual-band shared-aperture planar antenna array. By combining a patch antenna for the Ku-band and a cavity antenna for the Ka-band, a simple and single-fed network is realized. The proposed antenna element is further extended to a linear array antenna and a sequentially rotated array antenna. The implemented sequentially rotated array antenna exhibited a measured impedance bandwidth of 17.4–19.7 GHz (12.4%) and 27.0–29.0 GHz (7.1%). Moreover, the proposed sequentially rotated array antenna demonstrated measured peak gains of 13.7 dBi for right-hand circular polarization in the Ku-band receiver and a measured peak gain of 15.6 dBi for left-hand circular polarization in the Ka-band transmitter, making it highly suitable for satellite communication.

1. Introduction

Satellite communication has been widely utilized in various areas, including broadcasting, disaster rescue, tracking, maritime affairs, emergency, and safety as shown in Fig. 1 [1–4]. However, traditional frequency bands are insufficient for meeting the requirements of improved data rates and capacity. Therefore, it has become necessary to design higher-frequency bands to enhance data transmission speeds [5–23].

With the demand for space miniaturization and cost-effectiveness becoming increasingly apparent, many researchers have been investigating the design of dual-band antennas. In [5–8], a method of achieving dual-band operation involved combining two different antennas. However, this approach had spatial efficiency limitations, prompting further research on antennas that shared the same aperture [9–23]. Shared aperture antennas include designs that combine radiators from different frequency bands [9,10], however, such designs result in complex radiator structures. To overcome this complexity, shared-aperture antennas using multilayer substrates were explored, which proved to be more effective in utilizing space and simplifying the radiator structure compared to previous proposals [11–19]. However, a drawback of these antennas is the requirement of separate power feeds for each band, leading to isolation issues and increased complexity in the feeding network. This complexity can make the integration of antennas and integrated circuits (ICs) challenging. To address these challenges, antennas designed with the same radiators and feeding network have been investigated [20–23].

The antenna proposed in [20] forms a dual band using separate radiators and can radiate vertical and horizontal polarization in the Ku band and dual circular polarization in the Ka-band using four ports. The use of a hollow waveguide results in excellent antenna performance, however, it has the drawback of requiring mechanical processing and printed circuit board fabrication together. In [21], the antenna achieved dual-band operation in the K and Ka bands using dual dielectric resonators. Although the feeding network is simple, the use of a dielectric resonator makes it difficult to employ this antenna in low-profile applications. The antenna proposed in [22] is a dual-band patch antenna with increased gain using a metasurface. However, owing to the long distance between the radiator and the ground, it is unsuitable for integration with ICs. In [23], the antenna creates a dual-band using a semi-hexagonal half-mode substrate-integrated waveguide

* Corresponding author.
E-mail addresses: jeongwookkim@ajou.ac.kr (J.-W. Kim), dnjs4040@cau.ac.kr (S.-W. Oh), hanlimlee@cau.ac.kr (H.L. Lee).

https://doi.org/10.1016/j.aej.2024.06.029
Received 1 August 2023; Received in revised form 28 April 2024; Accepted 12 June 2024
Available online 25 June 2024

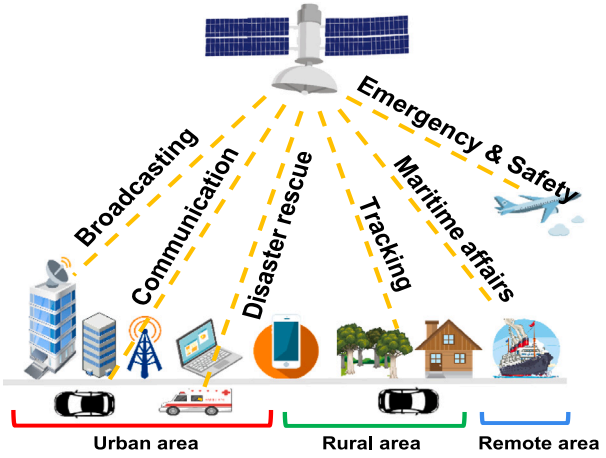

Fig. 1. Conceptual diagram of a satellite communication system.

Table 1
Detailed parameters of the proposed antenna element.

Parameter	Value (mm)	Parameter	Value (mm)
D1	4.1	R1	2.45
D2	4.05	R2	5.9
D3	1.35	G	17
ViaR1	0.4	ViaR2	0.25
ViaD1	2.65	ViaD2	4.95

cavity. However, the disadvantage is that the cavity structure results in a narrow bandwidth.

This paper presents a single-fed Ku/Ka dual-band shared-aperture planar antenna array for satellite communication. By utilizing a single feed, the proposed antenna overcomes the issue of low isolation and facilitates easy integration with a beamforming IC. The design facilitates a simple feed network, enabling both transmitting and receiving bands to be used within a single antenna element. Consequently, the number of antenna elements can be reduced by half. When this is combined with a dual-band beamforming IC, a reduction in the number of radio frequency ICs (RFICs) at the rear of the antenna is achieved, resulting in reduced power requirements and increased overall system efficiency. The proposed antenna element is expanded to a linear array antenna for linear polarization and a sequentially rotated array antenna for circular polarization. The Ku-band is used for the receiver band and the Ka-band is used for the transmitter band. In particular, the proposed sequentially rotated array antenna has a dual circular polarization for satellite communication applications, which is a right-hand circular polarization (RHCP) for the Ku-band and a left-hand circular polarization (LHCP) for the Ka-band. The designs of the proposed antenna element and array antenna were verified by implementation and measurement.

2. Antenna design

2.1. Antenna element design

The proposed antenna element, which is depicted in Fig. 2, comprises a combination of a circular patch antenna operating in the Ku-band with a circular ring cavity antenna designed for the Ka-band. The detailed parameters for the antenna are provided in Table 1. The antenna was fabricated utilizing a Taconic TLY-5 substrate (dielectric constant: 2.2, Tangent loss: 0.0009), with the integration of various layers using prepregs, RF04450B (dielectric constant: 3.7, Tangent loss: 0.004). Layer 1 comprises a circular patch and a ring ground, optimized for Ku-band operation, while layer 2 incorporates an additional ring ground, and layer 3 features a circular ground, both tailored for Ka-band operation. Layer 4 serves as a full ground for the antenna and feeding network.

The design process of the proposed antenna element is illustrated in Fig. 3(a). The Type A antenna represents a general patch antenna with a circular ground on layer 3. Furthermore, the Type B antenna incorporates an additional ring ground added to layer 2, and the Type C antenna includes the ring ground designed on layer 1. The design process involves combining the circular ground and ring ground to create the cavity antenna.

The real and imaginary parts of the input impedance resulting from this design process are displayed in Fig. 3(b) and Fig. 3(c), respectively. At the Ku-band, the real part of the input impedance for the Type A antenna is close to 50 Ω, and the imaginary part is close to 0 Ω. Introducing the ring ground on layer 2 of the Type B antenna results in the real part of the input impedance in the Ka-band remaining close to 50 Ω, while the imaginary part approaches 0 Ω because of capacitance, with only a minor change in the input impedance at the Ku-band. By placing the ring ground on layer 1 of the Type C antenna, the peak points of the input impedance are split into two points, with the real part of the input impedance close to 50 Ω, and the imaginary part close to 0 Ω. Consequently, as shown in Fig. 3(d), the reflection coefficient of the Type C antenna has a wider impedance bandwidth than the other types of antennas.

The simulated reflection coefficient based on parameter changes in the ring grounds and circular ground of each layer is depicted in Fig. 4. Fig. 4(a) shows the simulated reflection coefficient according to the radius of the ring ground on layer 1. As the radius of the ring ground on layer 1 ($D1$) increases, the resonant frequency of the Ku-band remains stable, while the resonant frequency of the Ka-band increases. To achieve a wide impedance band at the Ka-band, $D1$ was selected as 4.1 mm. Fig. 4(b) illustrates the simulated reflection coefficient with the change in the radius of the ring ground of layer 2 ($D2$). Similar to $D1$, as the radius of the ring ground on layer 2 ($D2$) increases, the resonant frequency of the Ka-band increases. For achieving a wide impedance band at the Ka-band, $D2$ was selected as 4.05 mm. Fig. 4(c) presents the simulated reflection coefficient according to the change in the radius of the circular ground ($D3$) on layer 3. As $D3$ increases, the resonant frequency of the Ku-band decreases, while the resonant frequency of the Ka-band increases and splits into two resonant frequencies. For a wide impedance band, $D3$ was selected as 1.35 mm. From the parameter study, it is evident that the size of the conductor pattern on each layer significantly affects the reflection coefficient. Moreover, the proposed antenna element was optimized to cover the frequency range of 17.9–20.1 GHz (12%) for the Ku-band and 27.9–31.1 GHz (11%) for the Ka-band. Both bands exhibited a wide bandwidth of 2.0 GHz or more.

The simulated electric field in the YZ plane of the proposed antenna element is depicted in Fig. 5. At 18.0 GHz, the electric field distribution resembles that of a general patch antenna, as depicted in Fig. 5(a). Two radiating slots are formed between the patch radiator and the circular ground on layers 3 and 4, allowing the electric field to be inserted into the ground on these layers. However, at 28.0 GHz, the radiating slots are formed near the ring cavities, resulting in the resonance of the electric field occurring at the edges of the circular cavity, as shown in Fig. 5(b).

The simulated radiation pattern and peak gain of the proposed antenna element are presented in Fig. 6. At 18.0 GHz, the radiation pattern resembles that of a general patch antenna, as shown in Fig. 6(a). The gain at the XZ plane is 5.9 dBi, and the 3-dB beamwidth is 75°. The cross-polarization within the beamwidth is below −18 dBi. Similarly, at the YZ plane, the gain is 5.95 dBi, and the 3-dB beamwidth is 109°, with cross-polarization within the beamwidth below −20 dBi. At 28.0 GHz, the radiation pattern takes a different shape, as depicted in Fig. 6(b). The gain at the XZ plane increases to 9.65 dBi, with a 3-dB beamwidth of 70°. The cross-polarization within the beamwidth is

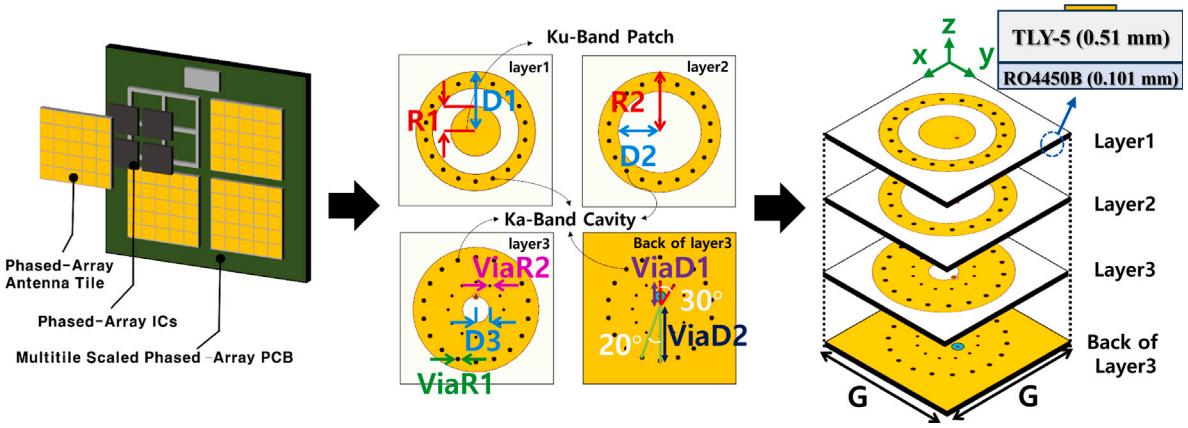

Fig. 2. Proposed antenna element.

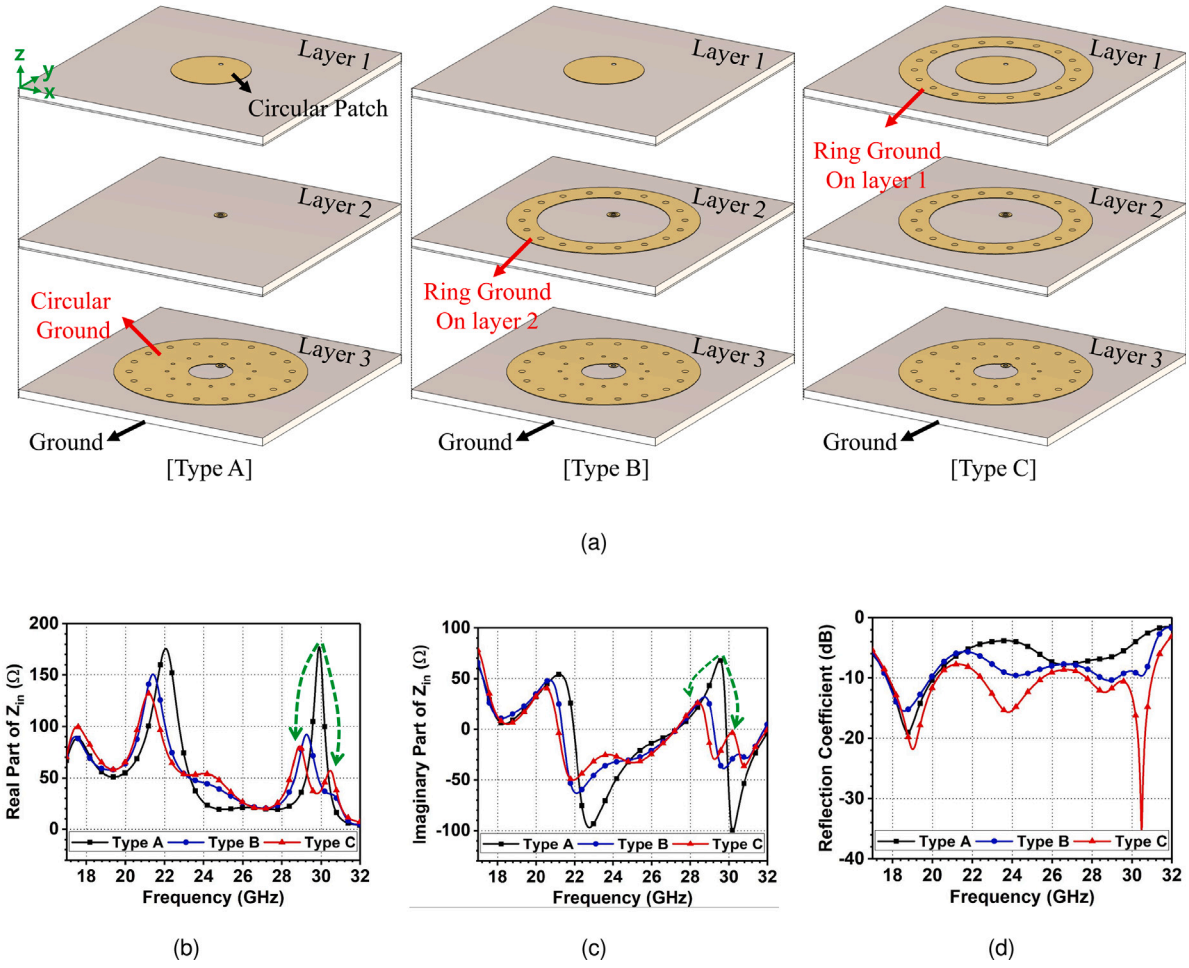

Fig. 3. (a) Design process of the proposed antenna element, (b) simulated real part of input impedance, (c) simulated imaginary part of input impedance, and (d) simulated reflection coefficient.

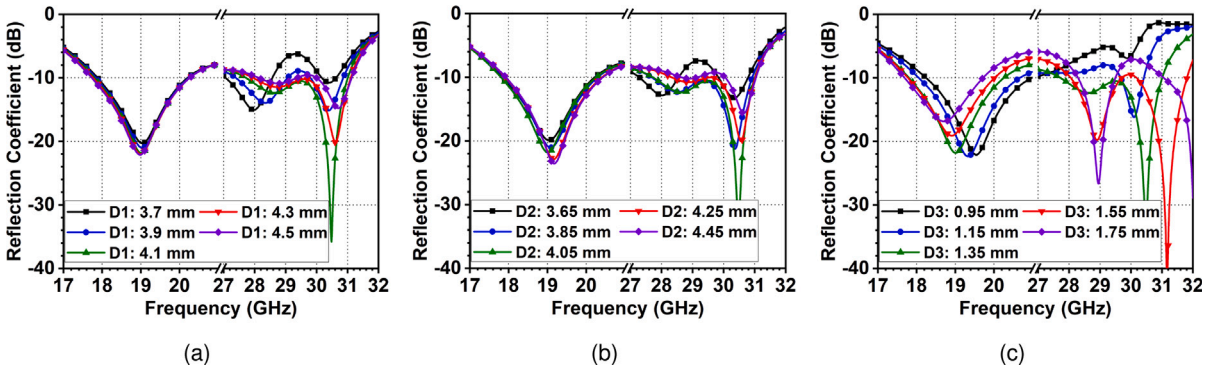

Fig. 4. Simulated reflection coefficient of the proposed antenna element according to (a) D1, (b) D2, and (c) D3.

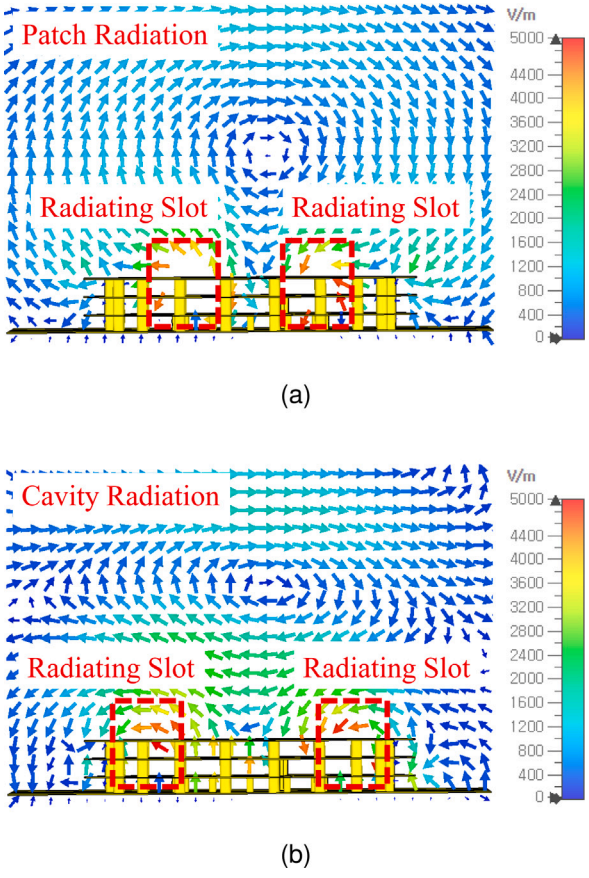

Fig. 5. Simulated electric field in the YZ plane of the proposed antenna element, (a) 18.0 GHz, and (b) 28.0 GHz.

below −3.0 dBi. Similarly, at the YZ plane, the gain reaches 9.65 dBi, and the 3-dB beamwidth narrows to 45°, with cross-polarization within the beamwidth below −7.0 dBi. The peak gain of the proposed antenna element at the Ku-band increases as the frequency increases, from 5.9 to 7.89 dBi at the XZ plane and from 5.95 to 8.36 dBi at the YZ plane. At the Ka-band, the peak gain ranges from 9.65 to 10.1 dBi at the XZ plane and from 9.65 to 10.2 dBi at the YZ plane.

2.2. Array antenna design

The proposed linear 1 *x* 4 array antenna is shown in Fig. 7. The feeding network is designed using a Wilkinson divider. The reflection coefficient of the proposed linear array antenna is presented in Fig. 8. Antenna1 and antenna4 have similar reflection coefficients and antenna2 and antenna3 have similar reflection coefficients. The reflection coefficient is under −10.0 dB from 17.9–20.0 GHz (11.1%) and 28.0–30.5 GHz (8.55%).

The simulated radiation pattern at 19.0 GHz is shown in Fig. 9(a). At this frequency, the gain at the XZ plane is 12.6 dBi, with a 3-dB beamwidth of 19°. The cross-polarization within the beamwidth is below −12.0 dBi. Similarly, at the YZ plane, the gain is 12.6 dBi, and the 3-dB beamwidth is 49°, with cross-polarization below −22.0 dBi. At 29.0 GHz, as shown in Fig. 9(b), the radiation pattern changes. The gain at the XZ plane increases to 15.7 dBi, with a 3-dB beamwidth of 13°. The cross-polarization within the beamwidth is below −7 dBi. Additionally, at the YZ plane, the gain reaches 15.6 dBi, with a 3-dB beamwidth of 40°, and cross-polarization below −10.0 dBi. The peak gain of the proposed antenna element at the Ku-band ranges from 11.0 to 12.6 dBi at the XZ plane and from 11.2 to 12.9 dBi at the YZ plane. At the Ka-band, the peak gain varies from 14 to 15.6 dBi at the XZ plane and from 14.4 to 15.9 dBi at the YZ plane.

The proposed sequentially rotated 2 *x* 4 array antenna, specifically designed for circular polarization in satellite communication applications, is depicted in Fig. 10. The array antenna is sequentially rotated to achieve RHCP for the Ku-band receiver and LHCP for the Ka-band transmitter. This circular polarization is accomplished using Wilkinson dividers, with a 1 *x* 4 Wilkinson divider employed for RHCP in the Ku-band and a 1 *x* 4 Wilkinson divider utilized for LHCP in the Ka-band. The reflection coefficient of the proposed sequentially rotated array antenna remains below −10 dB from 18.0–20.0 GHz (10.5%) for the Ku-band and from 27.1–29.2 GHz (7.5%) for the Ka-band, as shown in Fig. 11.

The radiation pattern at 18.0 GHz is illustrated in Fig. 12(a). At this frequency, the RHCP gain at the XZ plane is 11.4 dBi, with a 3-dB beamwidth of 41°. The LHCP gain within the beamwidth is below −6.0 dBi. Similarly, at the YZ plane, the RHCP gain is 11.2 dBi, and the 3-dB beamwidth is 47°, with the LHCP gain below −8.0 dBi. At 28.0 GHz, the radiation pattern changes as shown in Fig. 12(b). The LHCP gain at the XZ plane is 14.2 dBi, with a 3-dB beamwidth of 23 °, and the RHCP gain within the beamwidth is below −2.6 dBi. Additionally, at the YZ plane, the LHCP gain reaches 13.1 dBi, with a 3-dB beamwidth of 23°, and the RHCP gain within the beamwidth is below −2.6 dBi. As observed in Fig. 12(c), the peak gain of the proposed sequentially rotated array antenna at the Ku-band ranges from 11.2 to 14.1 dBi at both the XZ and YZ planes. Moreover, the axial ratio of the proposed antenna at the Ku-band varies from 0.5 to 1.2 dB at the XZ plane and

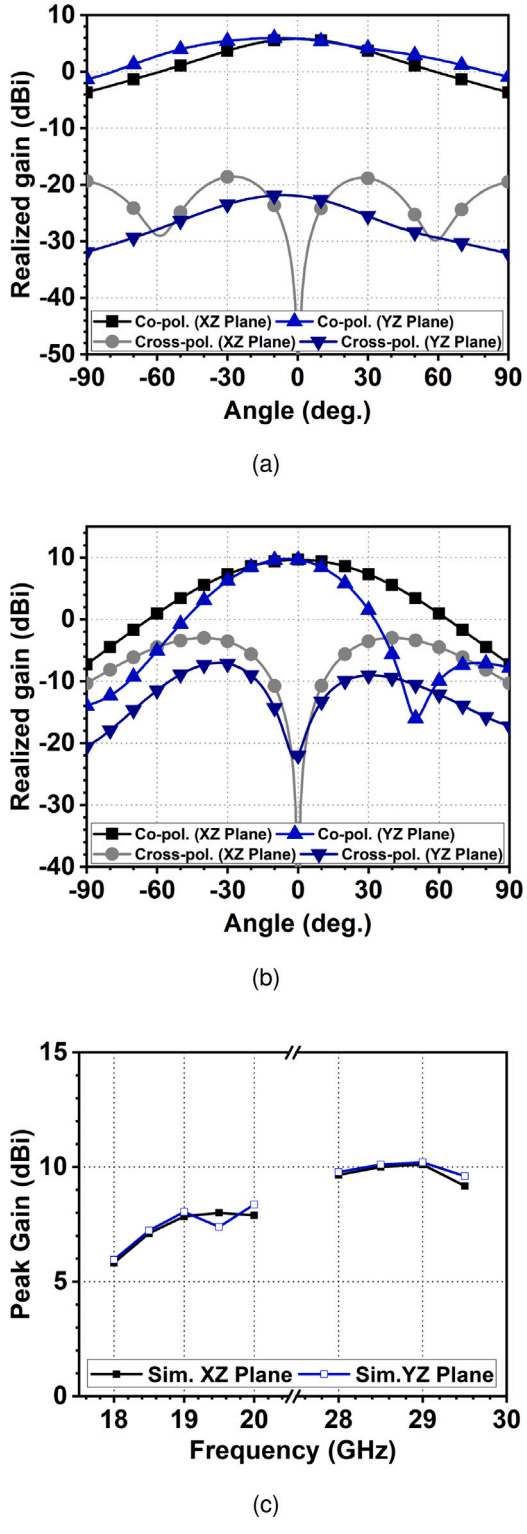

Fig. 6. Simulated radiation pattern of the proposed antenna element (a) at 18.0 GHz, (b) at 28.0 GHz, and (c) s simulated peak gain of the proposed antenna element.

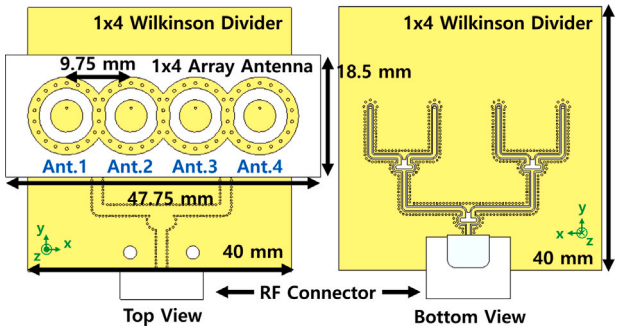

Fig. 7. Proposed linear array antenna.

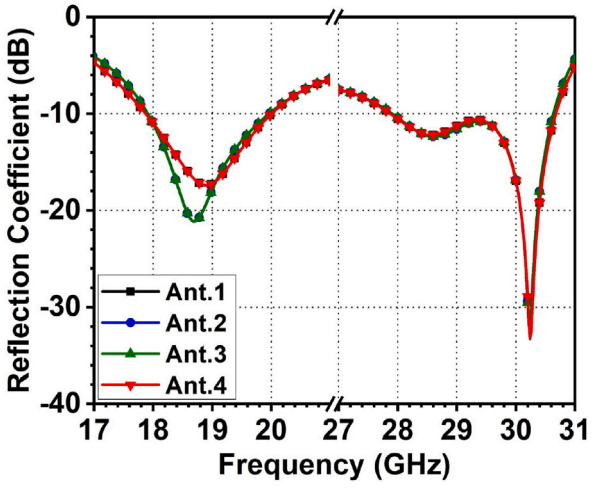

Fig. 8. Simulated reflection coefficient of the proposed linear array antenna.

from 0.4 to 1.55 dB at the YZ plane. At the Ka-band, the peak gain ranges from 12.6 to 15.3 dBi at the XZ plane and from 12.0 to 15.5 dBi at the YZ plane. Further, the axial ratio at the Ka-band varies from 1.9 to 2.1 dB at the XZ plane and from 2.19 to 2.7 dB at the YZ plane.

3. Fabrication and measurement

The implemented antenna element is displayed in Fig. 13. Further, Fig. 14 shows the simulation and measurement results of the reflection coefficient of the proposed antenna element. The measured impedance bandwidth is from 17.1 to 19.7 GHz (14.1%) and from 27.7 to 32.7 GHz (16.6%). The measured reflection coefficient follows a trend similar to the simulation results, confirming that both the Ku-band and Ka-band exhibit a wide bandwidth characteristics of 2.0 GHz or more. The agreement between simulation and measurement validates the effectiveness of the proposed antenna element design in achieving wide-band performance in both frequency bands.

The measured radiation pattern and peak gain of the implemented antenna element are illustrated in Fig. 15. In Fig. 15(a), at 18.0 GHz, the measured gain at the XZ plane is 5.6 dBi, with a measured 3-dB beamwidth of 71°. The measured cross-polarization within the beamwidth is below −13.0 dBi. Similarly, at the YZ plane, the measured gain is 5.3 dBi, and the measured 3-dB beamwidth is 140°, with cross-polarization within the beamwidth below −15.0 dBi. As shown in Fig. 15(b), at 28.0 GHz, the measured radiation pattern changes. The measured gain at the XZ plane increases to 9.4 dBi, with a measured 3-dB beamwidth of 54°, and the measured cross-polarization within the beamwidth is below −2.5 dBi. At the YZ plane, the measured gain is also 9.4 dBi, with a measured 3-dB beamwidth of 37°, and the measured cross-polarization within the beamwidth is below −6.0

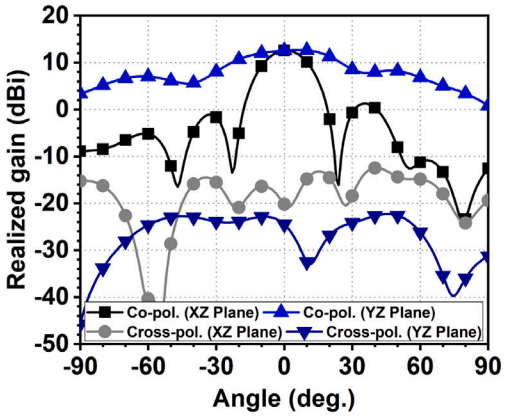

(a)

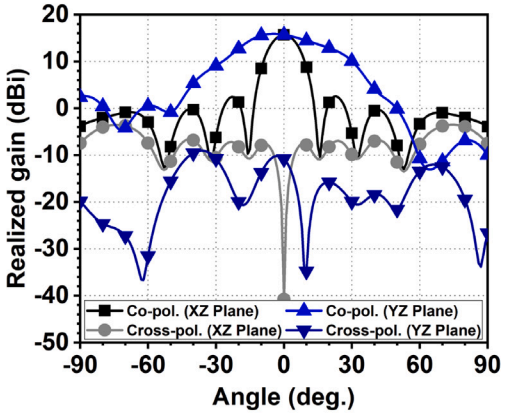

(b)

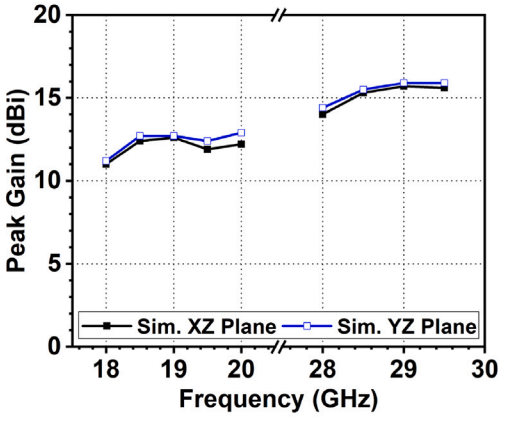

(c)

Fig. 9. Simulated radiation pattern of the proposed linear array antenna at (a) 19.0 GHz, (b) at 29.0 GHz, (c) Simulated peak gain of the proposed linear array antenna.

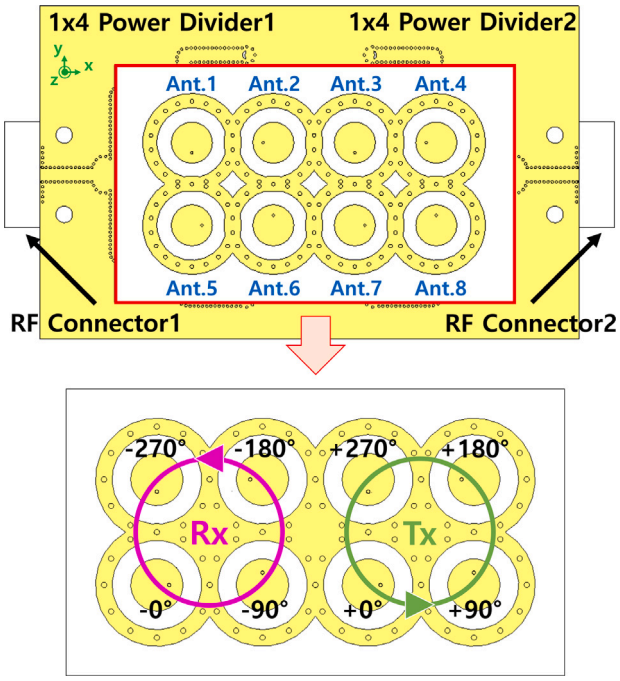

Fig. 10. Proposed sequentially rotated array antenna.

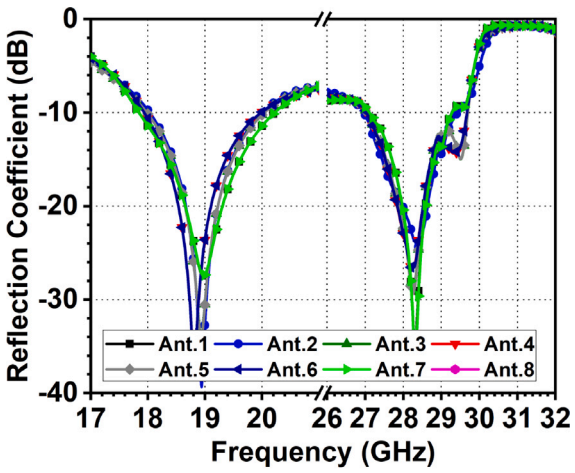

(a)

Fig. 11. Simulated reflection coefficient of the proposed sequentially rotated array antenna.

dBi. Fig. 15(c) summarizes the measured peak gain of the implemented antenna element. At the Ku-band, the measured peak gain ranges from 5.7 to 7.6 dBi at the XZ plane and from 5.6 to 7.8 dBi at the YZ plane. For the Ka-Band, the measured peak gain varies from 8.7 to 10.0 dBi at the XZ plane and from 9.2 to 9.8 dBi at the YZ plane.

The implemented linear 1 x 4 array antenna is displayed in Fig. 16. Further, Fig. 17 shows the simulation and measurement results of the reflection coefficient of the proposed antenna element. The measured band covered the ranges of 17.8–20.1 GHz (12.1%) and 28.0–30.5 GHz (8.55%). The measured reflection coefficient followed a trend similar to the simulation results, confirming the accuracy of the antenna design and the good impedance matching over the desired frequency ranges. The agreement between simulation and measurement further validates the performance of the proposed linear array antenna.

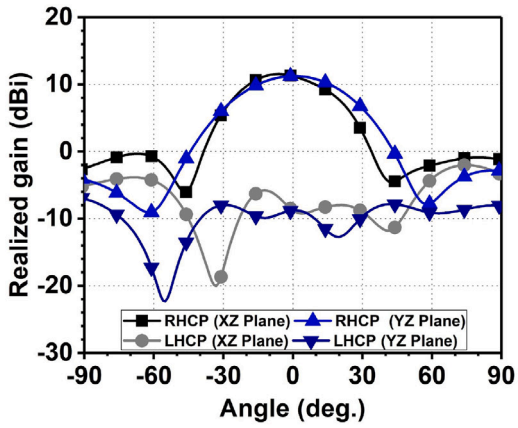

(a)

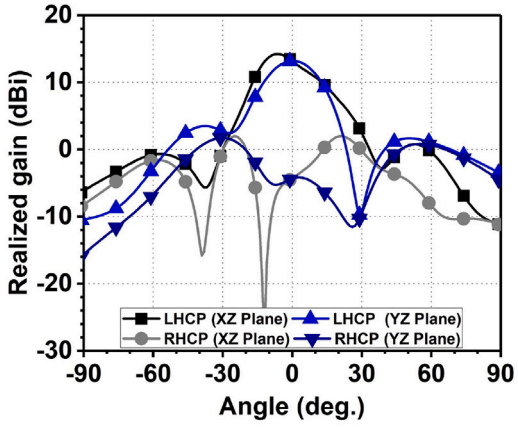

(b)

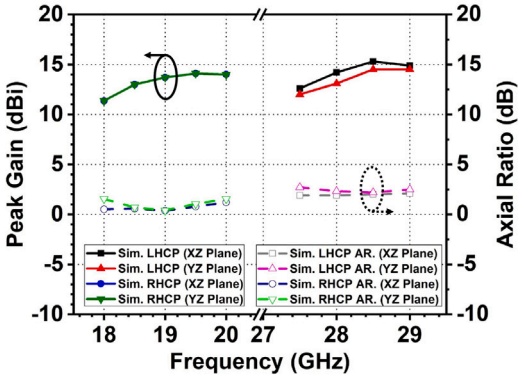

(c)

Fig. 12. Simulated radiation pattern of the proposed sequentially rotated array antenna (a) at 18.0 GHz, (b) at 28.0 GHz, (c) Simulated peak gain of the proposed sequentially rotated array antenna.

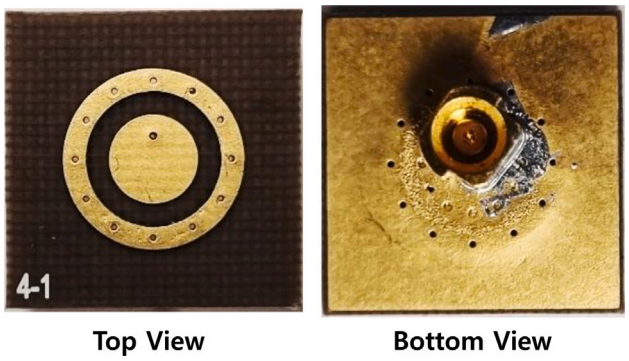

Fig. 13. Implemented antenna element.

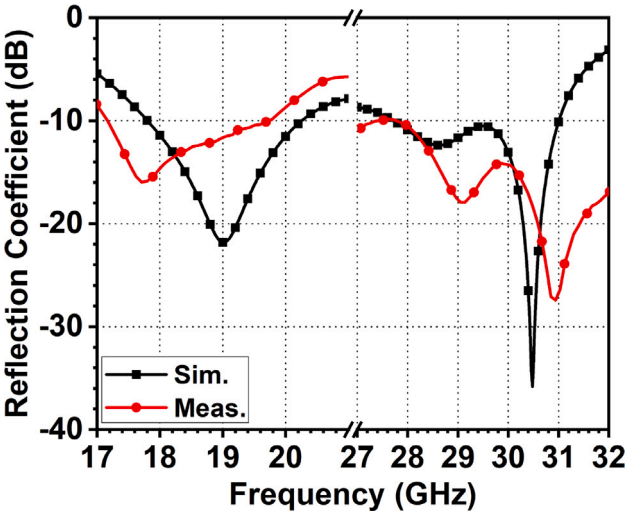

Fig. 14. Simulated and measured reflection coefficient of implemented proposed antenna element.

The measured radiation pattern and peak gain of the implemented linear 1 *x* 4 array antenna are presented in Fig. 18. At 19.0 GHz, the measured gain at the XZ plane is 12.7 dBi, and the measured 3-dB beamwidth at the XZ plane is 15° as shown in Fig. 18(a). The measured cross-polarization within the beamwidth is below −12.0 dBi. On the YZ plane, the measured gain is 12.3 dBi, with a measured 3-dB beamwidth of 101°, and the measured cross-polarization within the beamwidth is below −22.0 dBi. At 28.0 GHz, the measured radiation pattern changes as shown in Fig. 18(b). The measured gain at the XZ plane increases to 15.3 dBi, with a measured 3-dB beamwidth of 13°, and the measured cross-polarization within the beamwidth is below −5.0 dBi. At the YZ plane, the measured gain is 15.1 dBi, with a measured 3-dB beamwidth of 34°, and the measured cross-polarization within the beamwidth is below −7.0 dBi. Fig. 18(c) summarizes the measured peak gain of the implemented linear array antenna. At the Ku-band, the measured peak gain ranges from 11.2 to 12.7 dBi at the XZ plane and from 11.0 to 13.3 dBi at the YZ plane. For the Ka-band, the measured peak gain varies from 12.8 to 15.3 dBi at the XZ plane and from 12.9 to 15.1 dBi at the YZ plane.

The implemented sequentially rotated 2 *x* 4 array antenna is illustrated in Fig. 19. The implemented feeding networks consist of the 1 *x* 4 Wilkinson divider for RHCP in the Ku-band and the 1 *x* 4 Wilkinson divider for LHCP in the Ka-band. The array antenna is interfaced with the feeding networks through RF cables. Further, Fig. 20(a) presents the measurement results of the reflection coefficient for the implemented sequentially rotated array antenna. The measured bandwidth extends from 17.4–19.7 GHz (12.4%) and from 27.0–29.0 GHz (7.14%). These

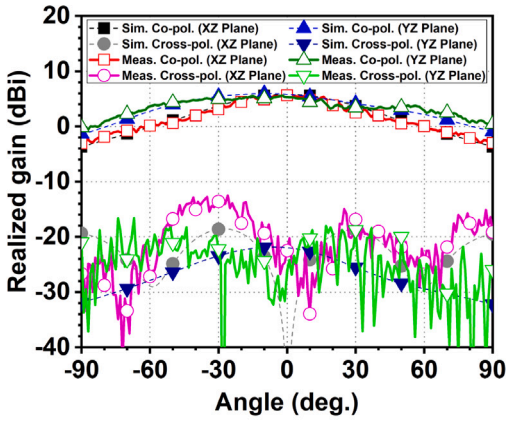

(a)

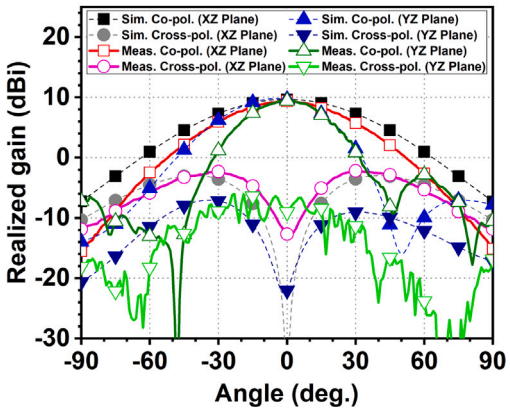

(b)

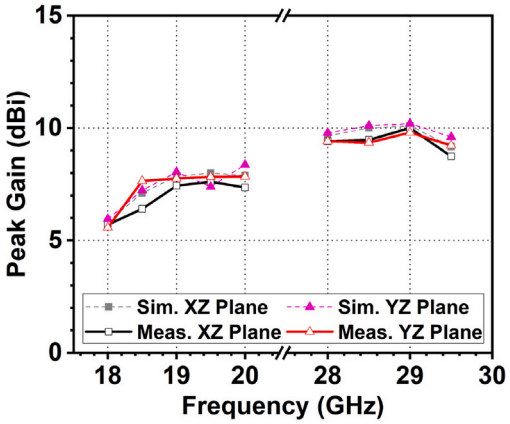

(c)

Fig. 15. Measured radiation pattern of the implemented antenna element (a) at 18.0 GHz, (b) at 28.0 GHz, (c) Measured peak gain of the implemented antenna element.

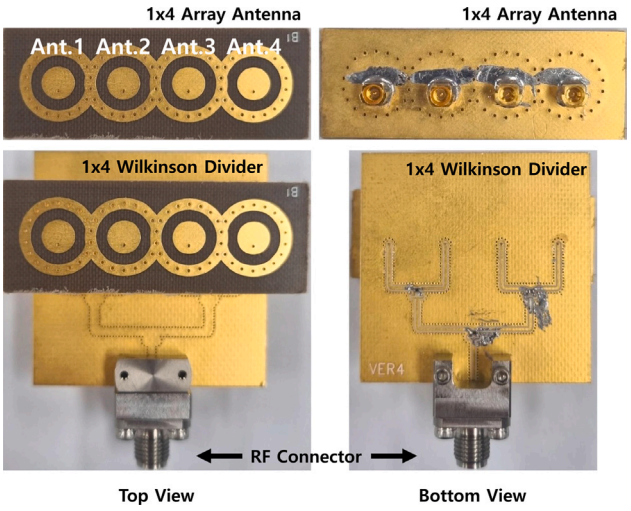

Fig. 16. Implemented proposed linear array antenna.

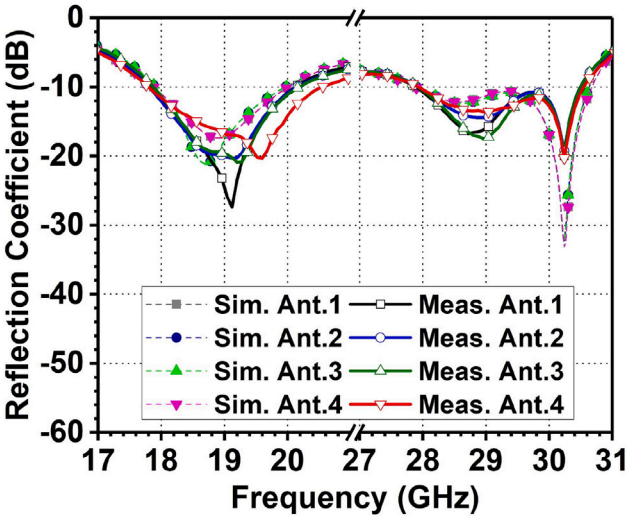

Fig. 17. Simulated and measured reflection coefficient of the implemented linear array antenna.

measured results validate the performance and wide impedance bandwidth characteristics of the antenna, making it suitable for satellite communication applications. In addition, the simulated and measured isolations of adjacent elements in the array are shown in Fig. 20(b), demonstrating values below −20 dB.

Next, the measured radiation pattern and peak gain of the implemented proposed sequentially rotated array antenna are shown in Fig. 21. As depicted in Fig. 21(a), the measured RHCP gain at the XZ plane is 10.7 dBi, and the measured 3-dB beamwidth at the XZ plane is 41°. The measured LHCP gain within the beamwidth is under −6.1 dBi. Similarly, the measured RHCP gain at the YZ plane is 11.4 dBi, and the measured 3-dB beamwidth at the YZ plane is 53°. The measured LHCP gain within the beamwidth is under −5.1 dBi. Fig. 21(b) depicts the measured radiation pattern at 28.0 GHz. The measured LHCP gain at the XZ plane is 14.5 dBi, and the measured 3-dB beamwidth at the XZ plane is 14°. The measured RHCP gain within the beamwidth is under −4.0 dBi. Moreover, the measured LHCP gain at the YZ plane is 12.8 dBi, and the measured 3-dB beamwidth at the YZ plane is 24°. The measured RHCP gain within the beamwidth is under −6.0 dBi. The measured peak gain of the implemented sequentially rotated array antenna at the Ku-Band ranges from 8.5 to 10.8 dBi, and the axial

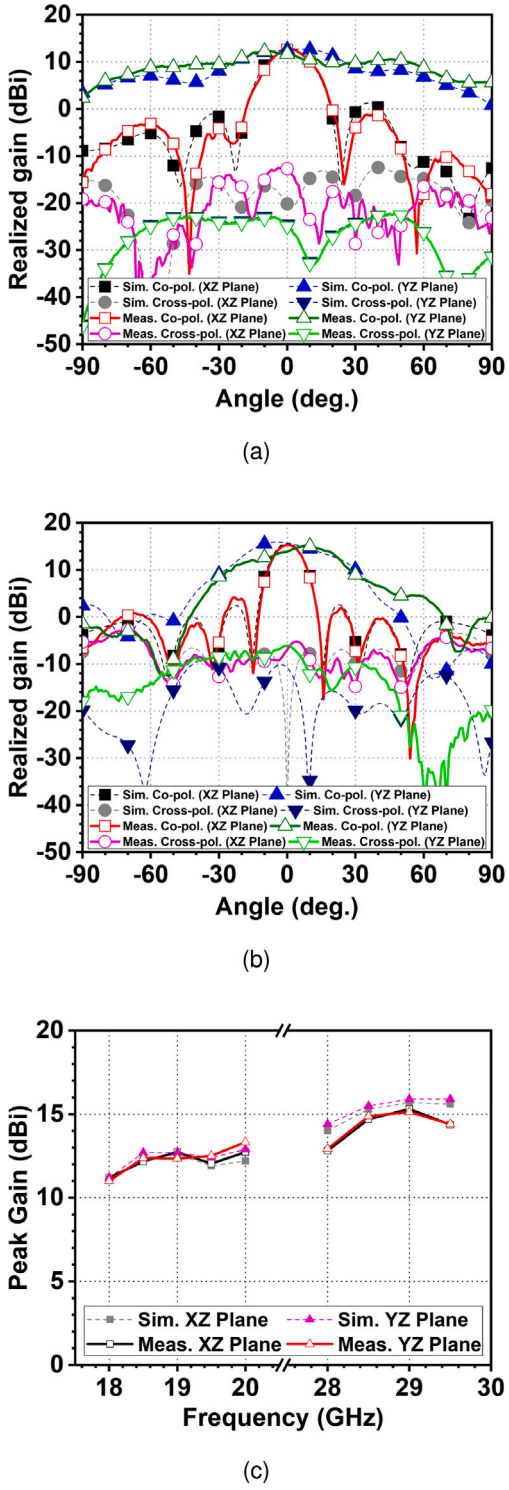

Fig. 18. Measured radiation pattern of implemented linear array antenna (a) at 19.0 GHz, (b) at 29.0 GHz, and (c) Measured peak gain of the implemented linear array antenna.

ratio varies from 0.6 to 2.1 dB. Furthermore, the peak gain of the implemented sequentially rotated array antenna at the Ka-band ranges from 11.8 to 15.6 dBi, and the axial ratio varies from 0.2 to 0.6 dB.

Table 2 provides a comparison with previously reported single-fed dual-band antennas. In [20], a metal waveguide-fed patch antenna featuring dual linear polarization (DLP) at the low band and dual circular polarization (DCP) at the high band was introduced. Despite its

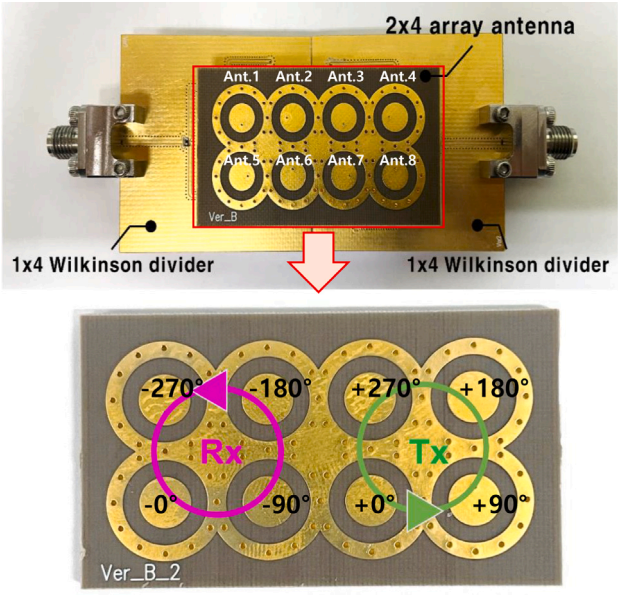

Fig. 19. Implemented sequentially rotated array antenna.

notable high gain performance, challenges arise from the implementation of the metal waveguide and the complexity of the feeding network. Additionally, the antenna's height of 2.8 λ_S, where λ_S represents the wavelength at the starting frequency of operation, renders it unsuitable for low-profile applications, unlike the proposed antenna, which stands at a mere 0.1 λ_S in height. In [21], a dielectric resonator antenna (DRA) designed with right-hand circular polarization (RHCP) at the low band and left-hand circular polarization (LHCP) at the high band was presented. However, the antenna's gain performance falls short compared to the proposed antenna element herein. Furthermore, the use of a dielectric resonator results in a thicker antenna height of 0.17 λ_S, further contrasting with the slender profile of the proposed antenna. The antenna proposed in [22] is a linear polarized patch antenna with an air gap. The antenna gain is enhanced by employing a metasurface. However, the antenna gain is still lower than that of the antenna element proposed herein, and the presence of the air gap between the radiator and the ground makes it unsuitable for integration with ICs. In [23], a cavity-fed patch antenna capable of circular polarization was proposed. However, the cavity structure restricts the bandwidth, resulting in a narrower bandwidth compared to the antenna element and array antenna proposed herein.

4. Conclusion

This paper proposes a single-fed Ku/Ka dual-band shared aperture planar antenna array for satellite communication. The antenna element combines a patch antenna for the Ku-band and a cavity antenna for the Ka-band, resulting in a simple and single-feed network. The proposed design is further extended to include a linear array antenna and a sequentially rotated array antenna. Remarkably, the implemented sequentially rotated array antenna exhibited a measured impedance bandwidth of 17.4–19.7 GHz (12.4%) and 27.0–29.0 GHz (7.1%). Additionally, the proposed sequentially rotated array antenna demonstrated a measured peak gain of 13.7 dBi for RHCP in the Ku-band receiver and a measured peak gain of 15.6 dBi for LHCP in the Ka-band transmitter. The proposed antenna offers several advantages, including higher gain and wider bandwidth, a simple radiator and feeding network, and a low-profile design compared to previously reported works, making it highly suitable for satellite communication applications.

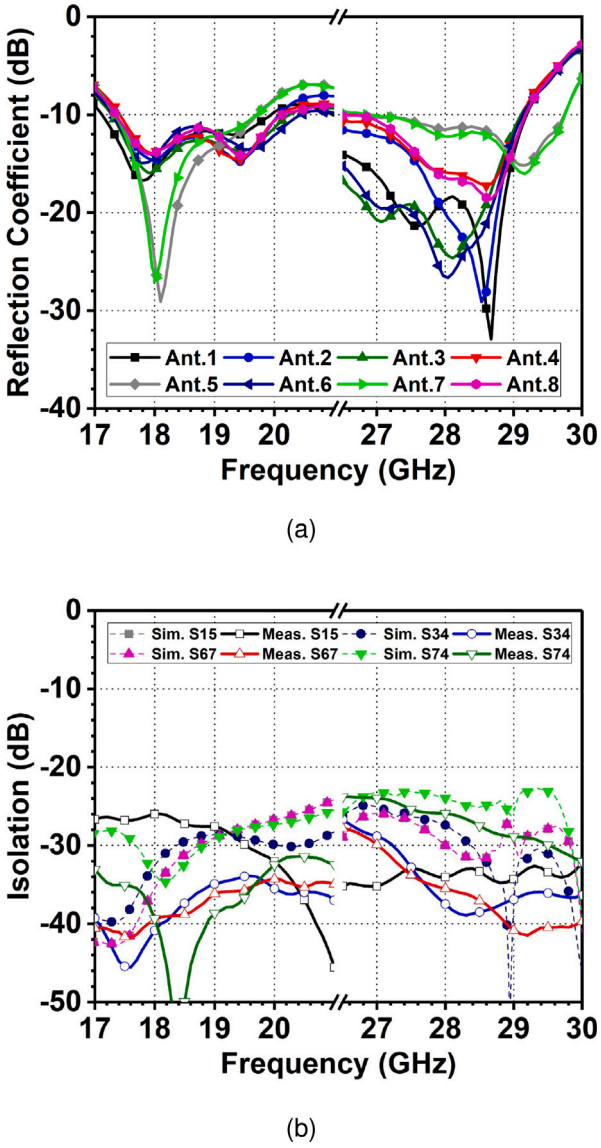

Fig. 20. (a) Measured reflection coefficient of the implemented sequentially rotated array antenna, (b) Simulated and measured isolation between adjacent elements in array.

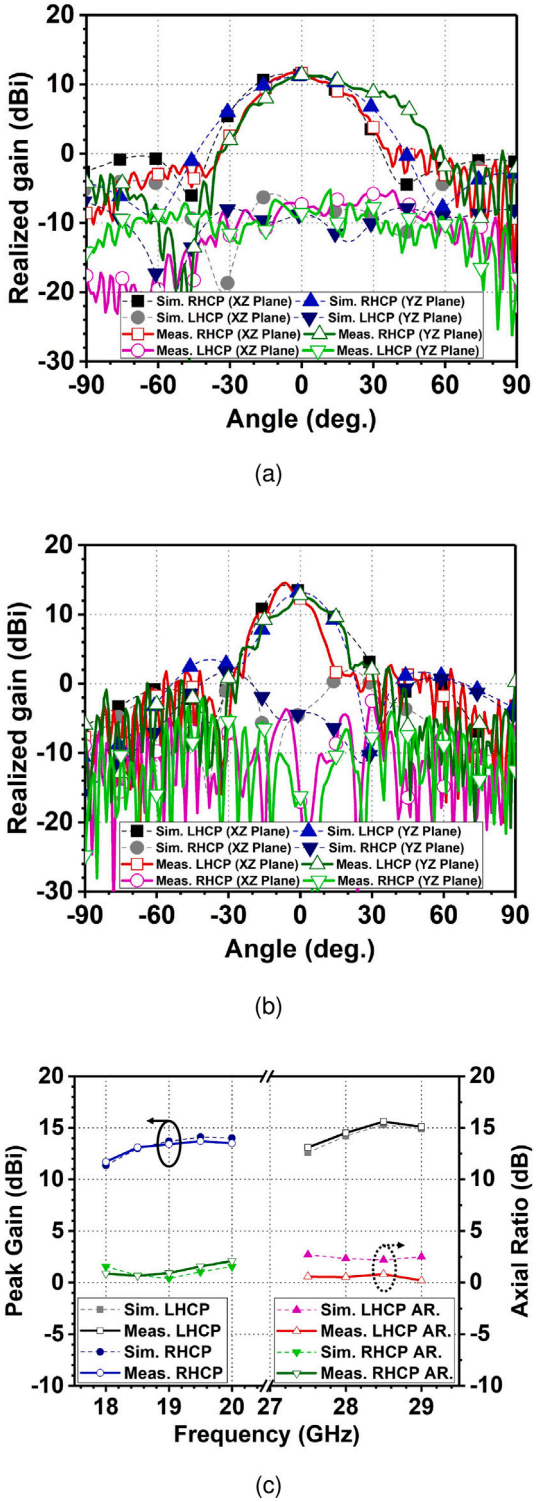

Fig. 21. Measured radiation pattern of proposed implemented sequentially rotated array antenna (a) at 19.0 GHz, (b) at 28.0 GHz, and (c) Measured peak gain of the implemented sequentially rotated array antenna.

CRediT authorship contribution statement

Jeong-Wook Kim: Conceptualization, Data curation, Formal analysis, Funding acquisition, Investigation, Methodology, Project administration, Resources, Software, Supervision, Validation, Visualization, Writing – original draft, Writing – review & editing. **Seung-Won Oh:** Conceptualization, Data curation, Formal analysis, Funding acquisition, Investigation, Methodology, Project administration. **Han Lim Lee:** Funding acquisition, Project administration, Resources, Supervision.

Declaration of competing interest

The authors declare that they have no known competing financial interests or personal relationships that could have appeared to influence the work reported in this paper.

Acknowledgments

This research was supported in part by the Development of Civil Military Technology Project from the Institute of Civil Military Technology Cooperation (ICMTC) under Grant 21-CM-RA-02, and in part by the Korea Institute for Advancement of Technology (KIAT) grant funded by the Korea Government (MOTIE) (P0017011, HRD Program for Industrial Innovation).

Table 2
Comparison with the previously reported single-fed dual-band antenna.

Reference	Antenna type	Center Freq. (GHz)	Bandwidth (%)	Peak gain	Polarization	Array number	Size
[20] (2023)	Waveguide-fed patch	16.0/33.8	19.4 /7.4	18.4/23.4 (dBic)	DLP/DCP	4 x 4/ 8 x 8	$4.3\lambda_s$x$4.3\lambda_s$x$2.8\lambda_s$
[21] (2021)	DRA	20.4/29.4	6.4 /12.6	6.6/8.2 (dBi)	RHCP/ LHCP	Single	$0.6\lambda_s$x$0.6\lambda_s$x$0.17\lambda_s$
[22] (2018)	Patch with air gap	5.5 /19.2	6.2/14.9	5.0/9.7 (dBi)	LP/LP	Single	–
[23] (2013)	Cavity-fed patch	8.0/9.5	1.3/3.7	9.2/8.8 (dBi)	RHCP/ LHCP	1 x 2	–
Proposed	Patch with cavity	18.4/30.2	14.1/16.6	7.8/10.1 (dBi)	LP/LP	Single	$1.0\lambda_s$x$1.0\lambda_s$x$0.1\lambda_s$
Proposed	Patch with cavity	19.0/29.3	12.1/8.6	13.3/15.3 (dBi)	LP/LP	1 x 4	$1.0\lambda_s$x$1.0\lambda_s$x$0.1\lambda_s$
Proposed	Patch with cavity	18.6/28.0	12.4/7.1	13.7/15.6 (dBi)	RHCP/ LHCP	2 x 2	$1.0\lambda_s$x$1.0\lambda_s$x$0.1\lambda_s$

References

[1] H. Zhao, et al., Ultra-wideband dual circularly polarized waveguide array antenna for K-and Ka-bands satellite communications, IEEE Antennas Wirel. Propag. Lett. (2023).
[2] Xin Chang, et al., Shared-aperture phased array antenna with codesigned near-field coupled circular polarizer loaded for K/Ka-band wide-angle satellite communication, IEEE Trans. Antennas and Propagation 70 (9) (2022) 7478–7490.
[3] Young-Bae Jung, Soon-Young Eom, Dual-band horn array design using a helical exciter for mobile satellite communication terminals, IEEE Trans. Antennas and Propagation 60 (3) (2011) 1336–1342.
[4] Sanghamitro Das, et al., A flat-panel 8 × 8 wideband K–/Ka–band dual circularly polarized phased array antenna for CubeSat communications, IEEE Trans. Antennas and Propagation (2023).
[5] Rui Sen Hao, et al., K-/Ka-band shared-aperture phased array with wide bandwidth and wide beam coverage for LEO satellite communication, IEEE Trans. Antennas and Propagation 71 (1) (2022) 672–680.
[6] Yan Ran Ding, Yu Jian Cheng, Ku/Ka dual-band dual-polarized shared-aperture beam-scanning antenna array with high isolation, IEEE Trans. Antennas and Propagation 67 (4) (2019) 2413–2422.
[7] Yan Ran Ding, et al., Dual-band shared-aperture two-dimensional phased array antenna with wide bandwidth of 25.0% and 11.4% at Ku-and Ka-band, IEEE Trans. Antennas and Propagation 70 (9) (2022) 7468–7477.
[8] Ai Hu Song, Yu Jian Cheng, Shared-aperture dual-polarized Ku-band and single-polarized Ka-band phased array antenna with scanning coverage enhancement, IEEE Trans. Antennas and Propagation 70 (11) (2022) 10426–10435.
[9] Simon Mener, Raphael Gillard, Langis Roy, A dual-band dual-circular-polarization antenna for Ka-band satellite communications, IEEE Antennas Wirel. Propag. Lett. 16 (2016) 274–277.
[10] Jin Fan Zhang, Yu Jian Cheng, K-/Ka-band planar shared-aperture beam-scanning array antenna for simultaneous transmitting and receiving low earth orbit satellite communication terminal, IEEE Trans. Antennas and Propagation (2023).
[11] Shengying Liu, et al., A dual-band shared aperture antenna array in Ku/Ka-bands for beam scanning applications, IEEE Access 7 (2019) 78794–78802.
[12] Bang Wei, et al., Ku/Ka dual-band shared-aperture leaky-wave antenna with fixed-frequency and wide-angle beam scanning based on ridged SIW, IEEE Trans. Antennas and Propagation (2023).
[13] Jian Ren, et al., Ku/Ka-band dual-frequency shared-aperture antenna array with high isolation using frequency selective surface, IEEE Antennas Wirel. Propag. Lett. (2023).
[14] Chun-Xu Mao, et al., Low-cost X/Ku/Ka-band dual-polarized array with shared aperture, IEEE Trans. Antennas and Propagation 65 (7) (2017) 3520–3527.
[15] Ali Imran Sandhu, et al., Radiating elements for shared aperture Tx/Rx phased arrays at K/Ka band, IEEE Trans. Antennas and Propagation 64 (6) (2016) 2270–2282.
[16] Yong Yang, Yong-Ling Ban, Qiang Sun, A X-/Ka-band linearly polarized low profile shared-aperture antenna array for satellite applications, IEEE Access 10 (2022) 105292-105302.
[17] Yilin Dong, et al., Compact shared-aperture dual-band dual-circularly-polarized waveguide antenna array operating at K/Ka-band, IEEE Trans. Antennas and Propagation 71 (1) (2022) 443–449.
[18] Rui Sen Hao, Yu Jian Cheng, Ya Fei Wu, Shared-aperture variable inclination continuous transverse stub antenna working at K-and Ka-bands for mobile satellite communication, IEEE Trans. Antennas and Propagation 68 (9) (2020) 6656–6666.
[19] Juqing Ran, et al., Dual-band dual-linearly/circularly polarized shared-aperture antenna for satellite communication systems, AEU-Int. J. Electron. Commun. 148 (2022) 154156.
[20] Juqing Ran, et al., Dual-band multi-polarized aperture-shared antenna array for Ku-/Ka-band satellite communication, IEEE Trans. Antennas and Propagation (2023).
[21] Hao Xu, et al., Single-fed dual-circularly polarized stacked dielectric resonator antenna for K/Ka-band UAV satellite communications, IEEE Trans. Veh. Technol. 71 (4) (2022) 4449–4453.
[22] Muhammad Asif, et al., Design of a dual band SNG metamaterial based antenna for LTE 46/WLAN and Ka-band applications, IEEE Access 9 (2021) 71553–71562.
[23] A. Vahid Sarani, Mohammad H. Neshati, Design investigation of dual-band dual-circularly polarized hybrid antenna array using semi-hexagonal HMSIW cavity, AEU-Int. J. Electron. Commun. 157 (2022) 154437.